Supporting Information

One-Pot Synthesis of Reduced Graphene Oxide/Metal (oxide) Composites

*Xu Wu, Yuqian Xing, David Pierce, Julia Xiaojun Zhao**

[a] Department of Chemistry, University of North Dakota, Grand Forks, ND58202, USA. Fax: 7017772331; Tel: 7017773610;

* Corresponding author, E-mail: Julia.zhao@und.edu

Electrochemical activity of RGO/Au nanocomposites. RGO has been widely used for electrochemical sensing due to its improved conductivity after reduction. Meanwhile, metal (oxide) nanoparticles have shown some electrocatalytic activity for the detection of biomolecules. Therefore, we evaluated the application of RGO/Au nanocomposites for the electrochemical detection of biomolecules. Compared with a GCE modified with GO and RGO, a GCE modified with RGO/Au nanocomposites showed higher conductivity and improved electron transfer rate, which yielded near-Nernstain behavior of the $[Fe(CN)_6]^{3-/4-}$ couple that was also diffusion controlled (Figure. S1).

Cyclic voltammetry was chosen to initially characterize the electrochemical activity of GO, RGO, and RGO/Au nanocomposite by using the $[Fe(CN)_6]^{3-/4-}$ couple in aqueous 1 M KCl as a redox standard. Figure. S1 A compares CV traces recorded at 50mV/s for a bare glassy carbon working electrode and the same GCE modified with GO, RGO or RGO/Au. The $[Fe(CN)_6]^{3-/4-}$ redox couple showed characteristically large (> 100 mV) CV peak separations (ΔE_p) and peak widths (E_p-$E_{p/2}$) for the bare GCE (Figure. S1 A, curve d). Such sluggish behavior of this couple is typical of many carbon surfaces[1] but it can be improved by modification.[2, 3] Addition of GO to the GCE surface (Figure. S1 A, curve c) increased the apparent rate of electron transfer ($\Delta E_p < 80$ mV) but it also reduced the measured current considerably. The later effect was likely caused by blocking of electrode surface by the low-conductivity GO. Addition of RGO to the GCE surface (Figure. S1 A, curve b) also improved electron transfer rate but, because of its higher conductivity, it did not have a blocking effect and manifested higher peak currents. Similarly, addition of

RGO/Au to the GCE surface (Figure. S1 A, curve a) yielded near-Nernstain behavior of the $[Fe(CN)_6]^{3-/4-}$ couple that was also diffusion controlled (Figure. S1 B and C).

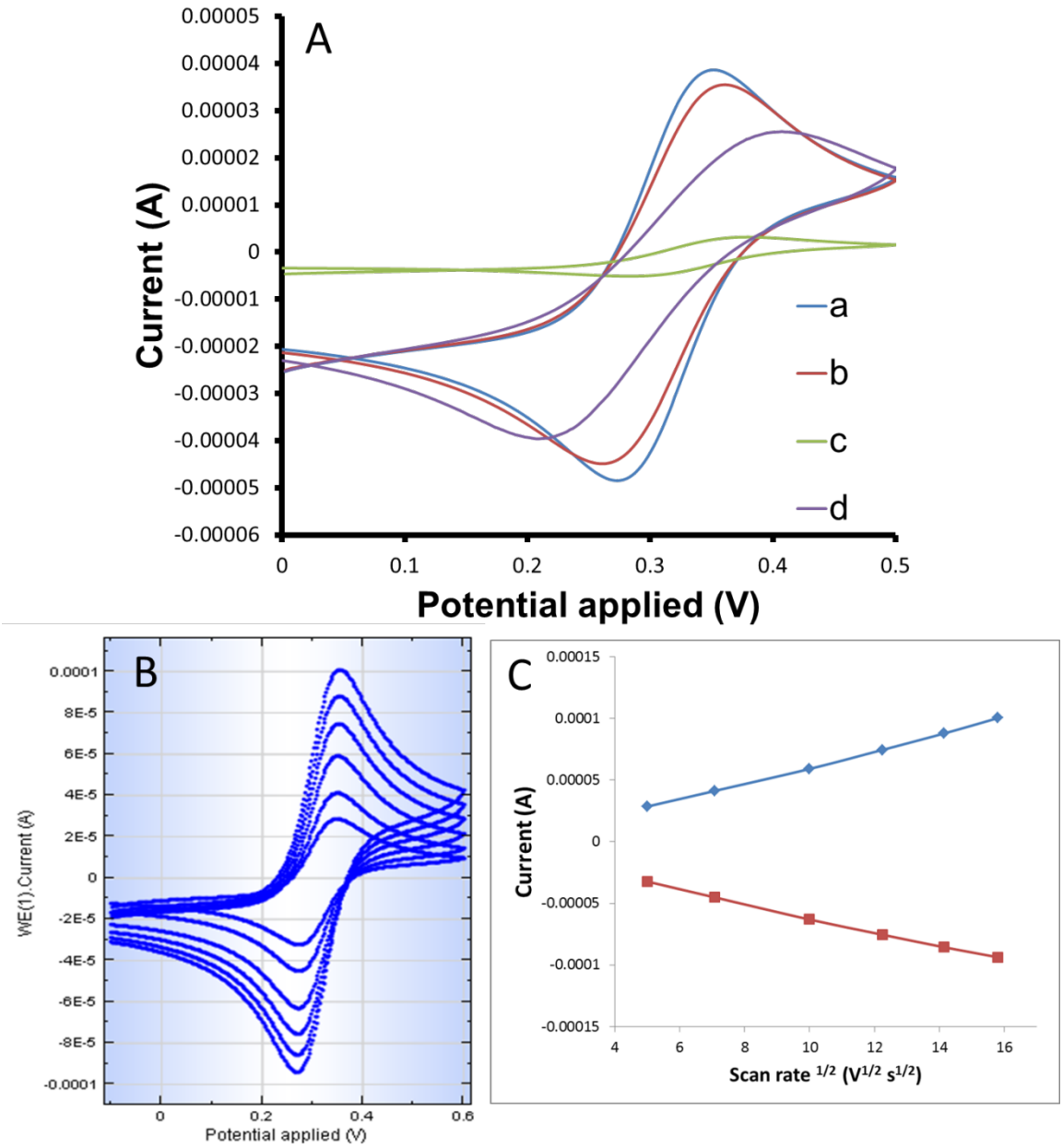

Figure S1. (A) The CV of RGO/Au-GCE (a), RGO-GCE (b), GO-GCE (c) and bare GCE (d), in the 5.0 mM $Fe(CN)_6^{3-/4-}$ solution. Scan rate: 50 mV/s; (B) CVs of RGO/Au-GCE in 5.0 mM

$Fe(CN)_6^{3-/4-}$ solution with different scan rate of 25, 50, 100, 150, 200 and 250 mV/s; (C) Plot of peak currents of RGO/Au-GCE versus square root of the scan rate.

L-AA detection. The electrochemical behavior of L-AA in 0.01 M PBS (pH 7.0) at a bare GCE, GO-GCE, RGO-GCE and RGO/Au-GCE was investigated using CV and DPV. As shown in Figure S2A, the L-AA oxidation was chemically irreversible with an anodic peak that changed significantly in shape and potential with different electrode modifiers. Bare GCE and GO-modified GCE yielded broad peaks at rather positive potentials (> +0.3 V) consistent with sluggish electron transfer. By comparison, the oxidation peaks with RGO- and RGO/Au-modified GCE were shifted to a much lower potential (ca. 0 V). The RGO/Au-modified GCE (Figure S2A, curve d) yielded a particularly narrow peak (E_p-$E_{p/2}$ ca. 70 mV) and enhanced peak current. These characteristics are consistent with electrocatalysis of the L-AA oxidation noted for other types of gold-modified electrodes. They also provide an enhanced signal for L-AA detection. To evaluate the sensitivity of the RGO/Au-modifier for detection of L-AA, DPV was used for concentrations of L-AA ranging from 0.1 to 1.0 mM in 0.01 M PBS. As shown in Figure S2C, background-subtracted peak oxidation current (I'_{pa}) was centered near 0 V and increased linearly below 1 mM with a sensitivity of 4.234 μA/mM (R^2 = 0.9973) L-AA (Figure S2D).

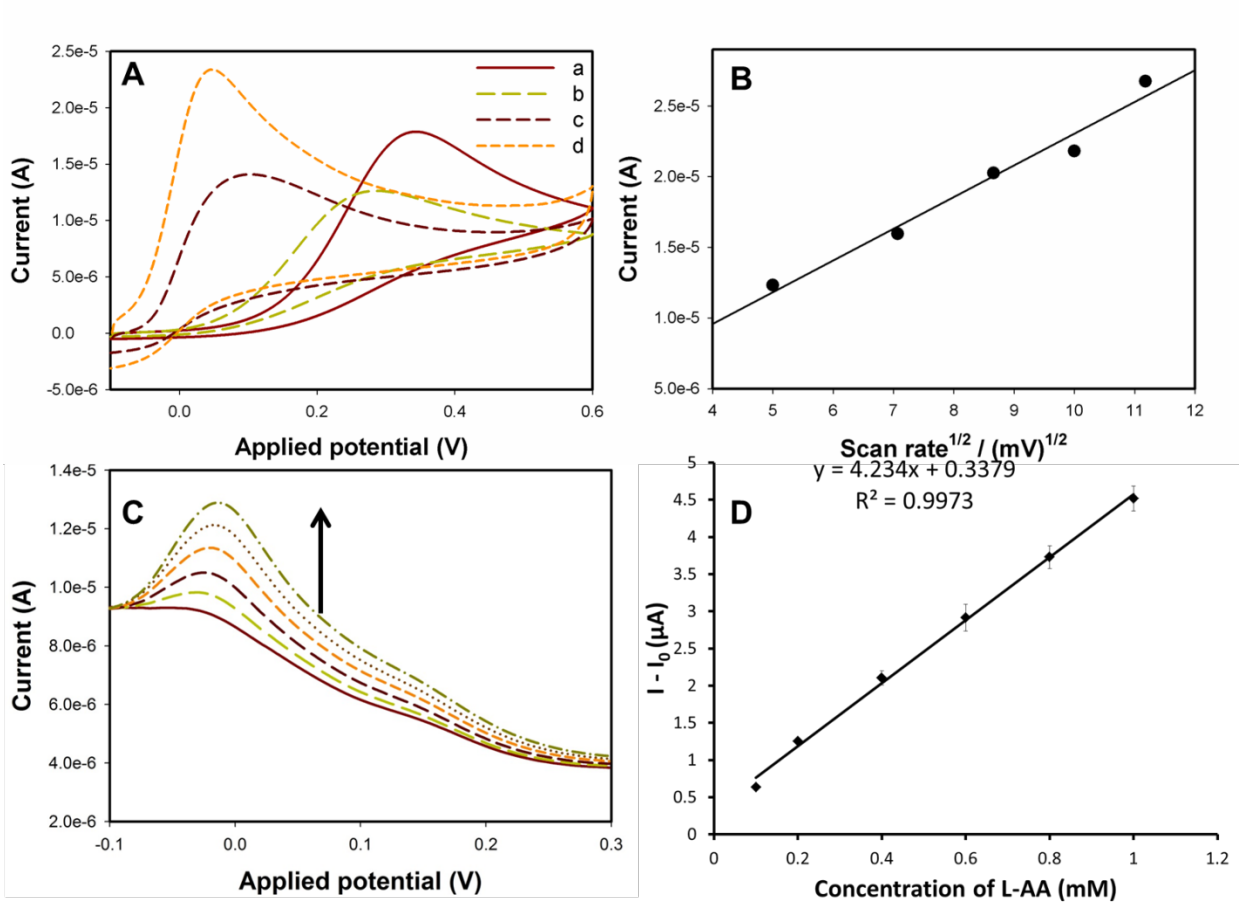

Figure S2. (A) CVs of the bare-GCE (a), GO-GCE (b), RGO-GCE (c) and RGO/Au-GCE (d) in 0.01 M PBS (pH 7.0) containing 1 mM L-AA. Scan rate: 50 mV/s; (B) Plot of oxidation peak of RGO/Au-GCE versus square root of the scan rate in 0.01 M PBS (pH 7.0) containing 1 mM L-AA; (C) DPV curves of RGO/Au-GCE in 0.01 M PBS (pH 7.0) containing different concentrations of L-AA (0.1, 0.2, 0.4, 0.6, 0.8 and 1.0 mM); (D) Plot of oxidation currents versus different concentration of L-AA at -0.014 V. I: oxidation peak current in the presence of L-AA; I_0: oxidation peak current in the absence of L-AA. Inset shows: the calibration curve of oxidation peak current response versus concentration of L-AA in the linear range of 0.1 - 1.0 mM.

DA detection. The CV and DPV behaviors of the RGO/Au-GCE for the DA detection were also investigated. As shown in Figure S3A, RGO/Au-GCE showed the highest peak currents compared to bare GCE, GO-GCE, and RGO-GCE, which indicated that the RGO/Au-GCE had the better catalytic activity and higher surface area (Figure S3A, d). Different from the CV behavior of L-AA (Figure S2A) and UA (Figure S4A), the DA showed a more chemically reversible process on the surface of RGO/Au-GCE. The anodic and cathodic peak currents were related to the square root of scan rate (Figure S3B), which showed that the electrochemical reaction of DA on the RGO/Au-GCE was a diffusion-controlled process. The sensitivity for DA detection was investigated with RGO/Au-GCE using DPV. As shown in Figure S3C and D, the current at *ca*. 0.16 V increased with the addition of DA in 0.01 M PBS. The oxidation peak current of DA was linear to the DA concentration at RGO/Au-GCE with a linear function $(I-I_0) = 0.6277\ C_{DA} + 0.1272$ ($R^2 = 0.9897$) in the range of 1.0 to 20 μM.

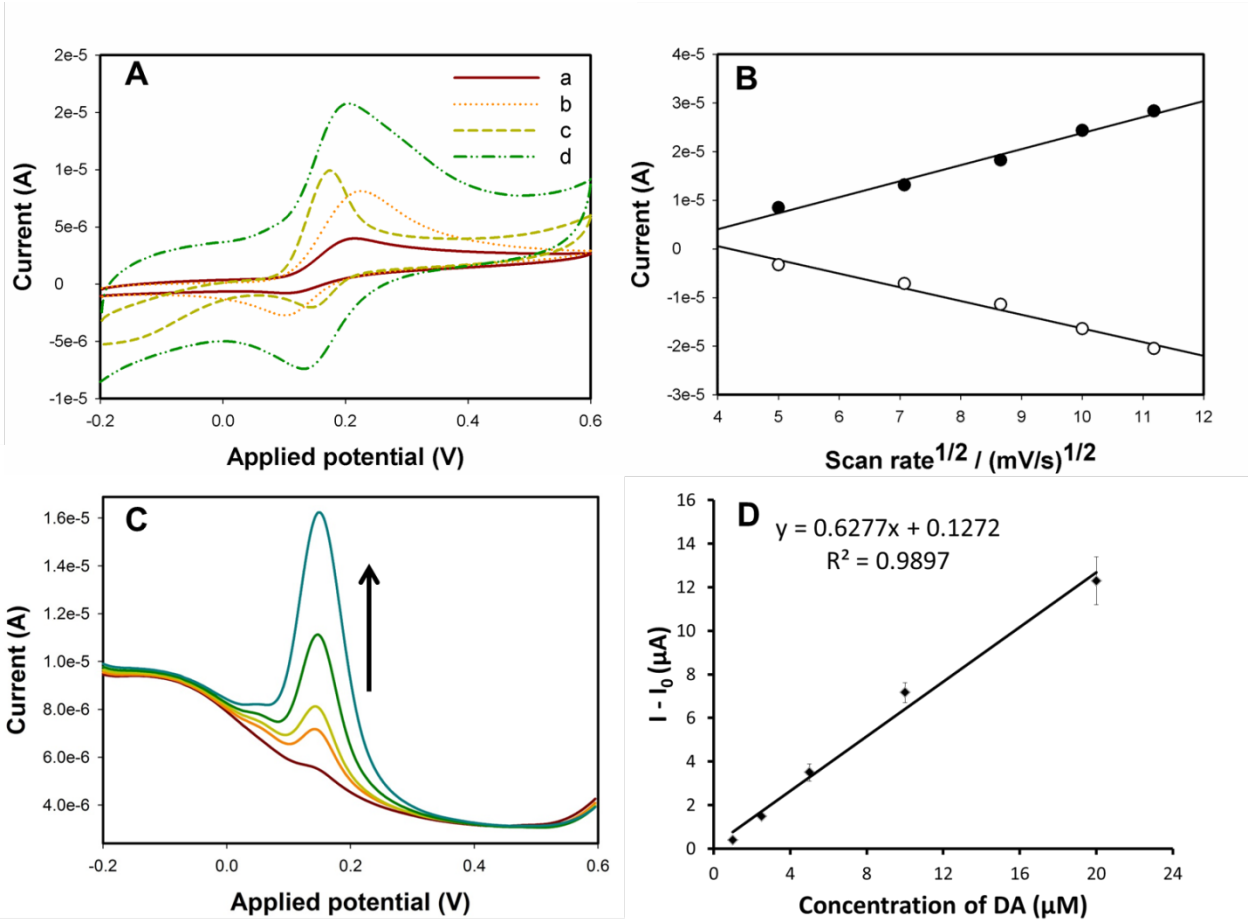

Figure S3. (A) CVs of the bare-GCE (a), GO-GCE (b), RGO-GCE (c) and RGO/Au-GCE (d) in 0.01 M PBS (pH 7.0) containing 160 μM DA. Scan rate: 50 mV/s; (B) Plot of oxidation peak of RGO/Au-GCE versus square root of the scan rate in 0.01 M PBS (pH 7.0) containing 80 μM DA; (C) DPV curves of RGO/Au-GCE in 0.01 M PBS (pH 7.0) containing different concentrations of L-AA (1.0, 2.5, 5.0, 10.0 and 20.0 μM); (D) Plot of oxidation currents versus different concentration of DA at 0.160 V. I: oxidation peak current in the presence of DA; I_0: oxidation peak current in the absence of DA. Inset shows: the calibration curve of oxidation peak current response versus concentration of DA in the linear range of 1.0-20.0 μM.

UA detection. The same process was carried out for the detection of UA using RGO/Au-GCE in 0.01 M PBS. As shown in Figure S4, UA showed an oxidation peak potential at *ca*. 0.32 V, which is a more negative potential than that for bare GCE and GO-GCE, and with the highest peak

current. Similar to the electrochemical behavior of L-AA and DA, UA showed a linear relationship between the oxidation peak current and the square root of scan rate (Figure S4B). The DPV peak current of UA was linear to the UA concentration at RGO/Au-GCE with a linear function ($I-I_0$) = 0.164 C_{UA} - 0.1863 (R^2=0.9866) in the range of 5-120 μM (Figure S4C and D).

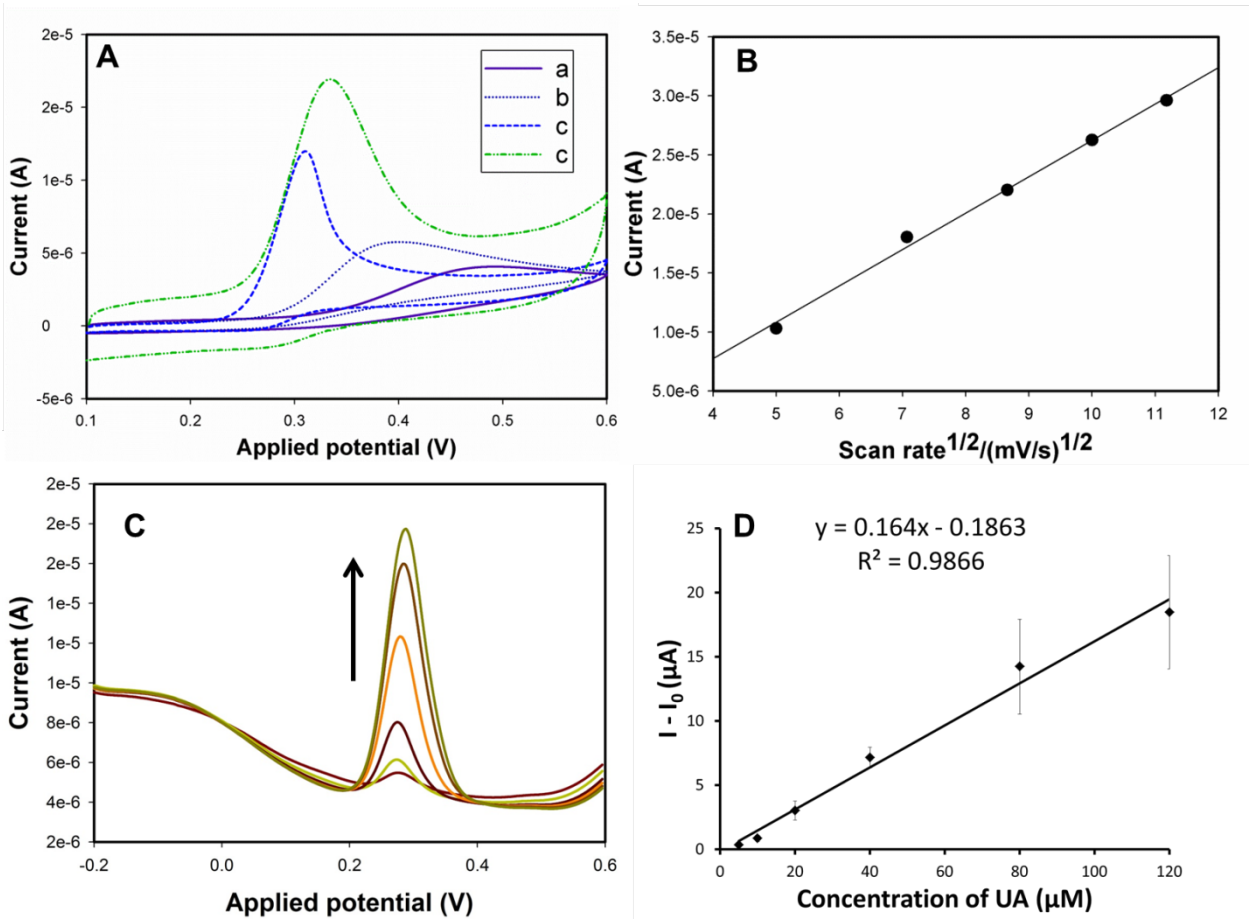

Figure S4. (A) CVs of the bare-GCE (a), GO-GCE (b), RGO-GCE (c) and RGO/Au-GCE (d) in 0.01 M PBS (pH 7.0) containing 200 μM UA. Scan rate: 50 mV/s; (B) Plot of oxidation peak of RGO/Au-GCE versus square root of the scan rate in 0.01 M PBS (pH 7.0) containing 200 μM UA; (C) DPV curves of RGO/Au-GCE in 0.01 M PBS (pH 7.0) containing different concentrations of L-AA (5, 10, 20, 40, 80 and 120 μM); (D) Plot of oxidation currents versus different concentration of UA at 0.290 V. I: oxidation peak current in the presence of UA; I_0: oxidation peak current in

the absence of UA. Inset shows: the calibration curve of oxidation peak current response versus concentration of UA in the linear range of 5-120 μM.

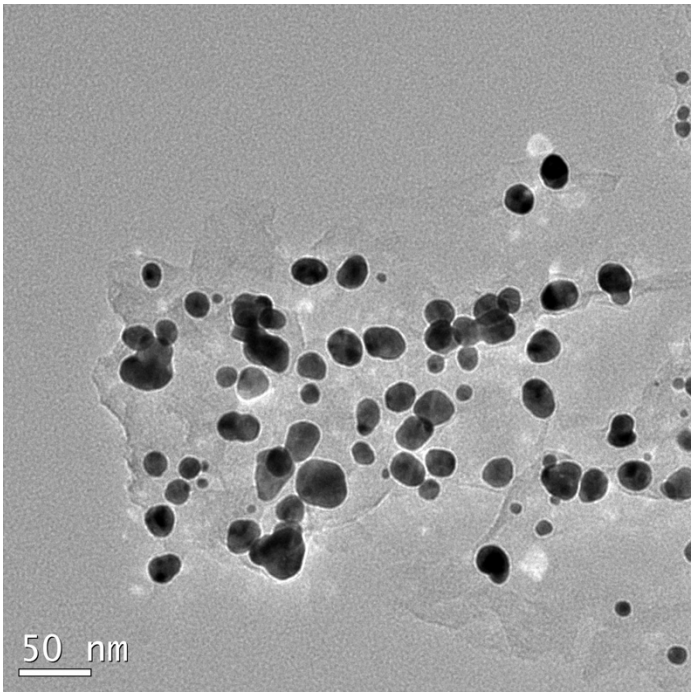

Figure S5. TEM image of RGO/Au nanocomposite after five measurements of L-AA.

References

1. Ruiyi, L.; Qianfang, X.; Zaijun, L.; Xiulan, S.; Junkang, L., Electrochemical Immunosensor for Ultrasensitive Detection of Microcystin-LR Based on Graphene–Gold Nanocomposite/Functional Conducting Polymer/Gold Nanoparticle/Ionic Liquid Composite Film with Electrodeposition. *Biosens. Bioelectron.* **2013**, *44*, 235-240.
2. Zhu, C.; Guo, S.; Fang, Y.; Dong, S., Reducing Sugar: New Functional Molecules for the Green Synthesis of Graphene Nanosheets. *ACS Nano* **2010,** *4*, 2429-2437.

3. Zhang, Z.; Chen, H.; Xing, C.; Guo, M.; Xu, F.; Wang, X.; Gruber, H.; Zhang, B.; Tang, J., Sodium Citrate: a Universal Reducing Agent for Reduction / Decoration of Graphene Oxide with Au Nanoparticles. *Nano Res*. **2011,** *4*, 599-611.